Magnetic Circuit Analysis of a Linear Switched Reluctance Motor

Amoros J. G.[1] , Andrada Gascón P.[2]

[1] Universitat Rovira i Virgili
Avinguda Països Catalans, 26
Tarragona, Spain
Tel.:+34 / 977-55 96 95,
Fax:+34 / 977-55 96 05
E-mail: jordi.garcia-amoros@urv.cat

[2] GAECE. Grup d'Accionamients Elèctrics amb Commutació Electrònica
Departament d'Enginyeria Elèctrica, EPSEVG-UPC
Víctor Balaguer s/n, 08800 Vilanova i la Geltrú, Spain
Tel.:+34 / 93 896 77 32;
Fax: +34 / 93 896 77 00
E-mail: pere.andrada@upc.edu

Acknowledgements

This research was supported by the Spanish Ministry of Education and Science and the European Regional Development Fund (DPI2006-09880).

Keywords

«Electrical machine», «Switched reluctance drive», «Linear drive», «Modelling»

Abstract

In this paper a magnetic circuit analysis has been developed to obtain flux linkage/current characteristics in aligned and unaligned positions for a Linear Switched Reluctance Motor. The model is based on lumped parameters and it takes into account the leakage pole flux and the end effects. The lumped parameter magnetic analysis proposed can be a useful tool for designing Linear Switched Reluctance Machines. The procedure has been verified using two dimensional finite element analysis and experimental measurements.

Introduction

Linear Switched Reluctance Motors (LSRMs) are an alternative to linear induction motors or permanent magnet synchronous motors. They are attractive because they only have concentrate windings on the stator or translator, they are ruggedly constructed and they have low expected manufacturing costs and a high fault tolerance [1]. They have recently been proposed as a propulsion system [2] for railway vehicles or vertical elevators [3].
LSRMs are the counterparts of rotary switched reluctance motors so it is very important during the design stage to predict the flux linkage-current-position characteristics and the magnetization curves, particularly in the aligned and unaligned positions. This is not an easy task because of the highly nonlinear behavior of the motor. One way to solve this problem is to use Finite Element (FE) analysis. Such an analysis would take a relatively long time because quite a number of solutions would be required at various translator positions and excitation levels. Another option is to develop an analytical model based on geometrical dimensions and the B-H curve of the magnetic material used. This lumped parameter magnetic circuit method is a good and fast approach for obtaining magnetization

curves in the aligned and unaligned position. In this paper a lumped magnetic circuit analysis that includes flux leakage and end winding leakage flux is applied to a four phase longitudinal double sided LSRM (Fig.1).

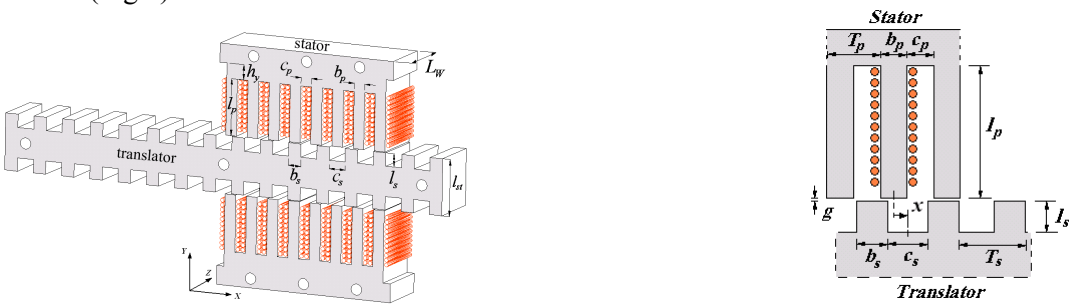

(a) (b)

Fig. 1: (a) 3D view of a double side LSRM and its main dimensions; (b) Details of the main dimensions

Lumped parameter magnetic circuit analysis

The main flux paths for aligned and unaligned positions in an LSRM are shown in Fig. 2. The main flux path encompasses four parts: stator yoke, stator pole, translator pole and air gap. Due to the length and tightness of stator poles, the model has to take into account the leakage pole flux. The analysis of the magnetic circuit is made by means of a lumped parameter model. From the main flux path shown in Fig. 2, a lumped parameter model (LPM) can be obtained for the equivalent magnetic circuit of the LSRM (Fig.3a).

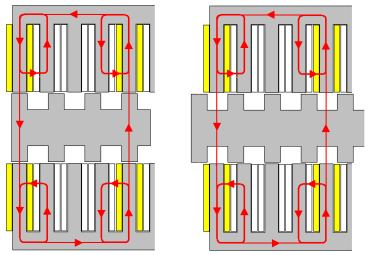

Fig. 2: Main flux paths for an LSRM: aligned (left) and unaligned (right)

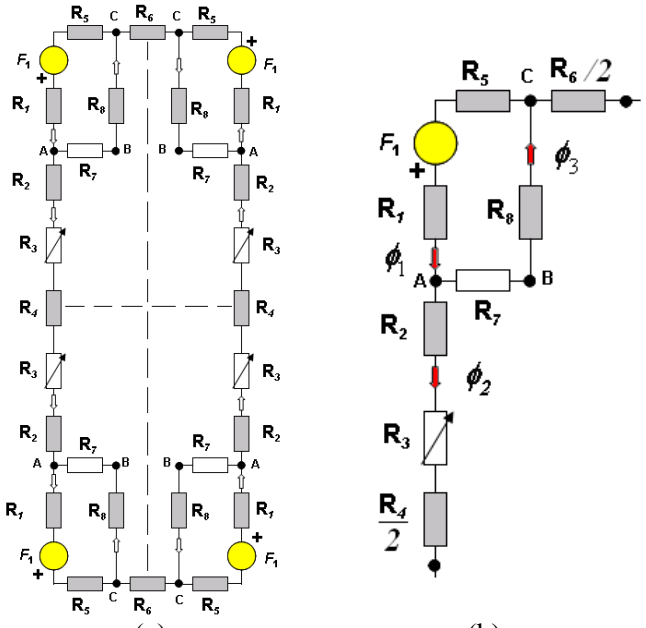

(a) (b)

Fig. 3: (a) Equivalent magnetic circuit; (b) Equivalent magnetic circuit per pole

The equivalent magnetic circuit is expressed in terms of reluctance. The shaded reluctances (see Fig. 3a) are non linear (ferromagnetic) and the white reluctances are linear (air). In order to model the leakage flux, the reluctance of the primary pole is divided into two reluctances, R_1 and R_2 (see Fig. 3b), and the primary pole flux is also divided into the fluxes Φ_1, Φ_2 .The fluxes depicted in Fig. 3b are the primary pole flux linked with the secondary flux (Φ_2) and the leakage pole flux (Φ_3). Equation 1 links the fluxes Φ_1, Φ_2 and Φ_3..

$$\phi_1 = \phi_2 + \phi_3 \tag{1}$$

In the same way, the reluctance of the yoke is divided into R_5 and R_6 which are crossed by flux Φ_1 and flux Φ_2 respectively. The remaining reluctances are crossed by flux Φ_2. The air gap reluctance $R_3(x)$ depends on translator position (x) (see Fig.1b), where $x=T_S/2$ for the aligned position and $x=0$ for the unaligned position. The distance between the aligned and unaligned positions (S) is given by:

$$S = \left(b_s + c_s\right)/2 \tag{2}$$

Table I: Effective length, sections and reluctances

Part	Effective length l (m)	Effective section S (m^2)	Reluctance R (H^{-1})
1	$\alpha_p \cdot l_p$	$b_p \cdot L_W$	$R_1 = \frac{\alpha_p \cdot l_p}{\mu_0 \cdot b_p \cdot L_W}$
2	$(1-\alpha_p) \cdot l_p$	$b_p \cdot L_W$	$R_2 = \frac{(1-\alpha_p) \cdot l_p}{\mu_0 \cdot b_p \cdot L_W}$
3	$l_3(x)$	$S_3(x)$	$R_3(x) = \lambda_3^{-1}(x)$
4	l_{st}	$b_s \cdot L_W$	$R_4 = \frac{l_{st}}{\mu_0 \cdot b_s \cdot L_W}$
5	$c_p + \pi \cdot b_p / 4 + h_y / 2$	$h_y \cdot L_W$	$R_5 = \frac{4 \cdot c_p + \pi \cdot b_p + 2 \cdot h_y}{4 \cdot \mu_0 \cdot h_y \cdot L_W}$
6	$2 \cdot T_P$	$h_y \cdot L_W$	$R_6 = \frac{2 \cdot T_P}{\mu_0 \cdot h_y \cdot L_W}$
7	c_p	$l_p \cdot L_W \cdot \alpha_p$	$R_7 = \frac{c_p}{\mu_0 \cdot \alpha_p \cdot l_p \cdot L_W}$
8	$\alpha_p \cdot l_p + h_y / 2$	$b_p \cdot L_W$	$R_8 = \frac{\alpha_p \cdot l_p + h_y / 2}{\mu_0 \cdot b_p \cdot L_W}$

The air gap flux tubes are basically made of straight lines and circumference arcs, in line with the methodology for estimating the permeance of probable flux paths [7]. Fig. 4 shows the main flux tubes for the aligned position. Fig. 5 shows the main flux tubes for the unaligned position. The parameter α_p presented in table I for the length of the parts 1 and 2, is defined as (see Fig. 4a - 5a):

$$\alpha_p = h_1 / l_p \tag{3}$$

In general, α_p depends on the shape of the flux tubes used and therefore depends on position (x).

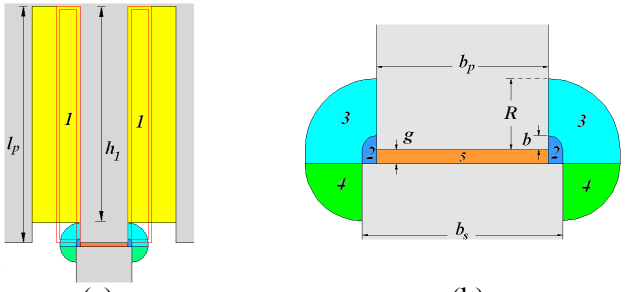

(a) (b)

Fig. 4: a) Air gap permeance flux tubes for the aligned position (x=S). b) Detail of flux tubes

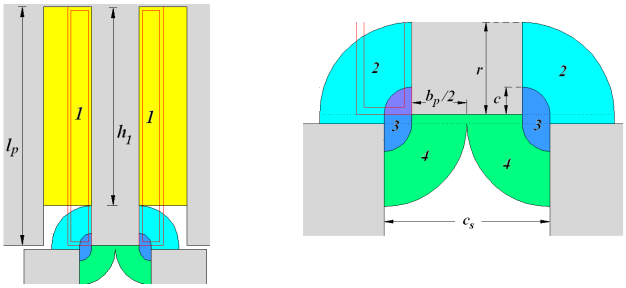

(a) (b)

Fig. 5: a) Air gap permeance flux tubes for the unaligned position (x=0). b) Detail of flux tubes

Where R=c_p (Fig.4b) and r=$c_p/(\pi \cdot l_p)$ (Fig.5b)

Table II: Effective length and sections for the air gap

	Effective gap length $l_3(x)$	Effective section $S_3(x)$
Aligned: x=S	g	$b_p \cdot L_W \cdot \left(\frac{\lambda_{3,a}}{\lambda_{3,5}} \right)$
Unaligned : x=0	$\mu_0 \cdot \frac{b_p \cdot L_W}{\lambda_{3,u}}$	$b_p \cdot L_W$

Where $\lambda_{3,a}$ and $\lambda_{3,u}$ are the air gap permeance for the aligned (Fig. 4b) and unaligned (Fig. 5b) positions respectively given by:

$$\lambda_{3,a} = \lambda_3(S) = \lambda_{3,5} + 2 \cdot \left[\lambda_{3,2} + \left(\lambda_{3,3}^{-1} + \lambda_{3,4}^{-1} \right)^{-1} \right] \tag{4}$$

$$\lambda_{3,u} = \lambda_3(0) = 2 \cdot \left(\lambda_{3,2} + \lambda_{3,3} + \lambda_{3,4} \right) \tag{5}$$

For intermediate positions (0<x<S), reference [4] shows a way of obtaining the air gap permeance. For brevity, the present study only models the aligned and unaligned positions.
The magneto motive force (*mmf*) applied (F_1=$N \cdot I$) to a phase winding is equal to the drop in the *mmf* along the path. Using *Ampere*'s circuital law in the circuit shown in Fig. 3b gives:

$$F_1 = \sum_{i=1}^{i=6} H_i \cdot l_i = H_1 \cdot l_1 + H_2 \cdot l_2 + H_3 \cdot l_3 + \frac{1}{2} \cdot H_4 \cdot l_4 + H_5 \cdot l_5 + \frac{1}{2} \cdot H_6 \cdot l_6 \quad (6)$$

Due to the non linearity of magnetic materials, equation (6) does not have a trivial solution and must be solved with an iterative algorithm using bi-section root searching (see Fig. 6 and appendix I).
In previous studies [5] [6], the air gap was modeled with *k* permeance tubes in parallel, and the equation (6) was solved for each permeance path. This means that (6) had to be solved for each permeance tube. In this study, the air gap permeance tubes are reduced to one equivalent permeance tube before solving equation 6. This reduces the number of iterations and therefore the computing time, although the computing time is quite reduced in both cases. The leakage pole flux is also modeled by the reluctances R_7 and R_8. (path A-B-C, see Fig. 3b). The *fmm* drop (θ_{AB}) of the leakage path A-B-C is much larger than (θ_{BC}) because the A-B part is air and the B-C part is non saturated ferromagnetic steel; therefore the *fmm* drop (θ_{BC}) can be considered negligible and this results in $\theta_{AC} \cong \theta_{AB}$.

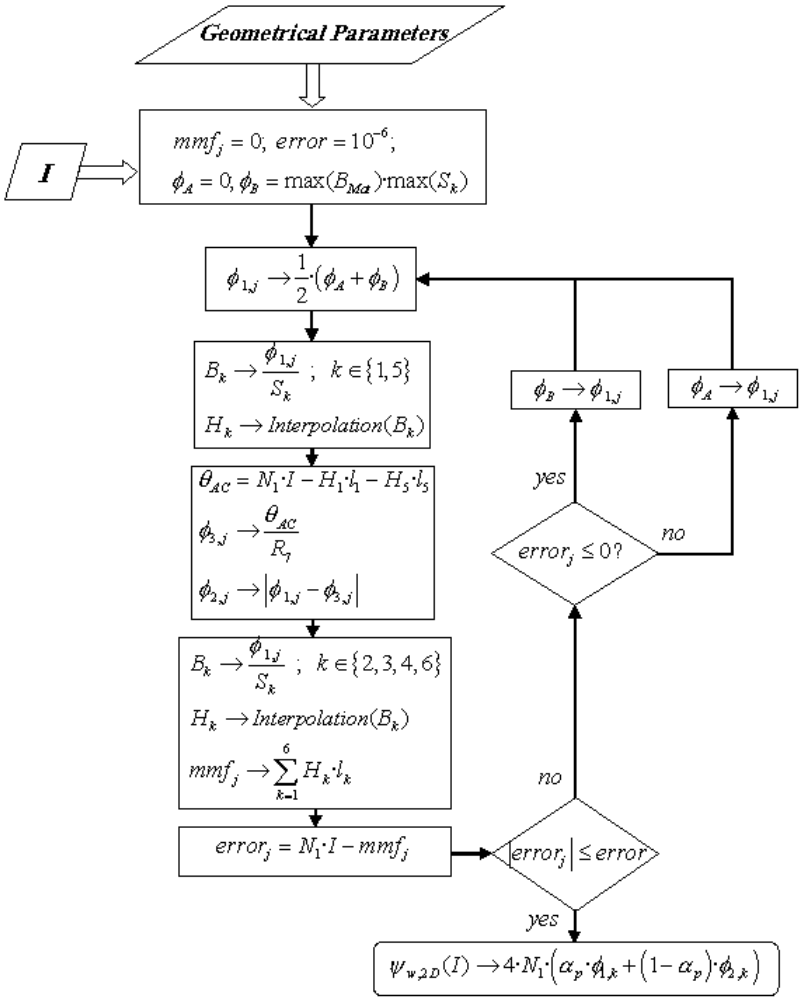

Fig. 6: Bi-section root finding algorithm for solving equation (6)

The algorithm described in Fig. 6 to solve (6) returns the pole flux (Ψ_p), the air gap flux (Ψ_s), the leakage flux (Ψ_d) and the winding flux (Ψ_w) linkages to the aligned and unaligned positions (see appendix I for details). The parameter that changes between these two positions is the air gap reluctance (see Table II).
In order to compute the inductance, the factor α_p determined in (3) is used to weight the air gap flux (Ψ_s) and the pole flux (Ψ_p) and thus obtain the flux linked by the winding (Ψ_w). The factor α_p is usually between 0.8 and 0.95.

End-effects: analytical approach

End effects are not included in 2D calculations despite the fact that these effects can increase the unaligned inductance by up to 20-30% [8]; in fact, the shorter the machine, the greater the increase. This reduces the energy conversion area predicted by 2D calculations and therefore lowers the performance calculations. End effects appear at the end of the lamination stack and are basically the consequence of extra flux linkages produced at the head or the end of the winding. This extra flux produces an axial fringing flux that, along with the steel imaging effect of the laminations, contributes to increasing these effects. End effects in 2D FEA are accounted for with the end-effects coefficient, K_{ee}, [9] depending on the current density (J) and position (x), given by:

$$\psi_{3D} = K_{ee} \cdot \psi_{2D} \qquad (7)$$

$$L_{3D} = K_{ee} \cdot L_{2D} \qquad (8)$$

Where Ψ_{2D} and L_{2D} are the flux linkage and the inductance obtained in 2D FEA and Ψ_{3D} and L_{3D} are the 3D flux linkage and the inductance approaches that account for the end effects and are most similar to the measured values. The end-effects coefficient, K_{ee}, is defined as:

$$K_{ee} = \left(1 + \frac{L_{end} \cdot K_{si}}{L_{2D}}\right) \cdot K_f \qquad (9)$$

Where, L_{end} is the end-winding inductance, K_{si} is a factor that affects L_{end} due to the steel imaging effect and K_f is the axial fringing factor. K_{si} can usually be omitted ($K_{si} = 1$) since its effect on L_{end} is generally less than 2%. From Fig.7, the end winding inductance, L_{end}, can be analytically deduced with classical methods [10].

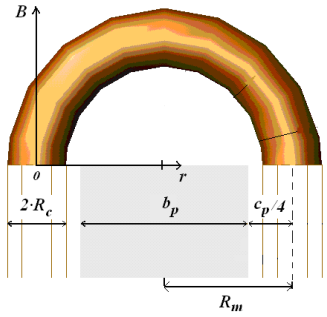

Fig. 7: Geometrical parameters for L_{end} calculation

Resulting in:

$$L_{end} = k \cdot N_1^2 \cdot \mu_0 \cdot (b_p + \frac{c_p}{2}) \cdot \ln\left(\frac{\sqrt{\pi} \cdot (b_p + \frac{c_p}{2})}{e^{-\frac{1}{4}} \cdot \sqrt{c_p \cdot l_p \cdot k_v}}\right) \qquad (10)$$

The axial fringing flux is due to the tendency of the magnetic flux to bulge out in the axial direction. This effect depends on the translator position and is stronger when the poles are fully unaligned (x=0) and is weaker when they are completely aligned (x=S). Therefore the axial fringing factor can be rendered by:

$$K_f(x) = 1 + \frac{2 \cdot g + l_s \cdot \left(1 + \cos\left(\pi \cdot x / S\right)\right)}{2 \cdot L_W} \qquad (11)$$

Verification and experimental results of finite elements analysis

The lumped parameter model (LPM) proposed is verified using two-dimensional finite element analysis (2D FEA) [11]. The LSRM translator moves from the aligned to the unaligned position for different excitation currents (Fig. 8). An LSRM prototype was built (see appendix II) and tested in order to evaluate the results obtained by means of the proposed procedure. A test setup was built to perform the experimental measurements (Fig. 9). The experimental flux linkage–current curves were obtained following the procedure described in [12]. Fig. 10 compares the results obtained by LPM, by 2D FEM and by measuring without including end effects (Fig.10a) and by measuring including end effects (Fig. 10b).

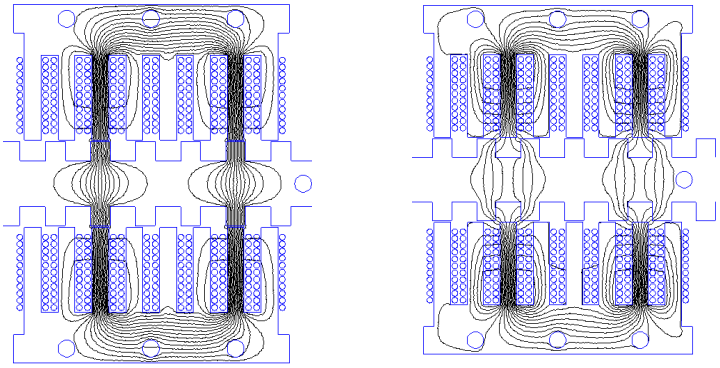

(a) (b)

Fig. 8: Flux plots from FEM analysis of the LSRM; a) Aligned b) Unaligned

Fig. 9: View of LSRM prototype and experimental setup

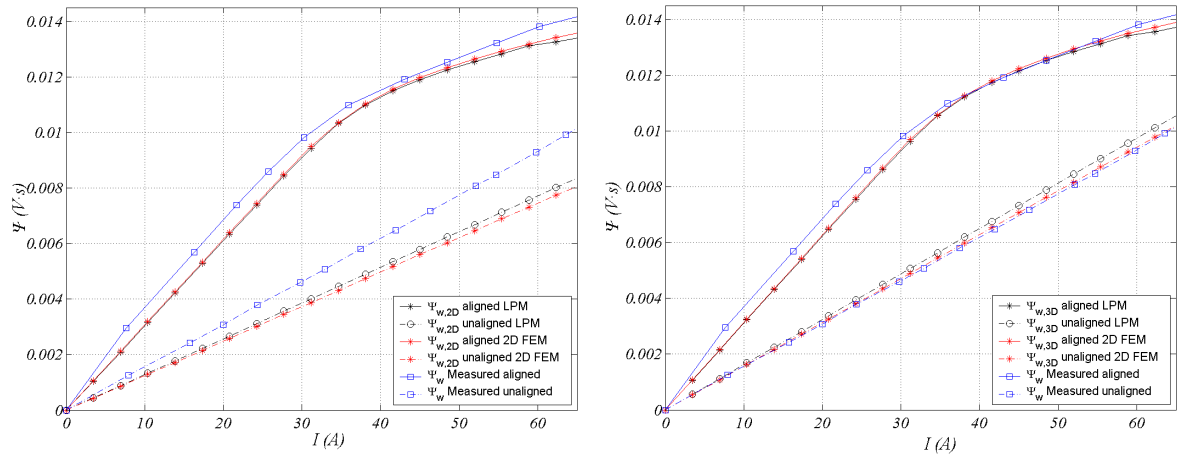

(a) (b)

Fig. 10: Comparison of results of LPM, 2D FEM and measurements a) without including end effects b) including end effects

Conclusion

A lumped magnetic circuit analysis that includes flux leakage is applied to a four phase double sided LSRM. The computational time for the lumped parameter magnetic circuit method is smaller than that of the 2D-FEA; therefore, it can be a useful tool for designing LSRMs. 2D-FEA and experimental results confirm that the lumped magnetic circuit analysis proposed can be a useful tool for optimizing the geometry of double sided LSRM.

References

[1] Boldea I., Nasar S A., "*Linear Electric Actuators and Generators*", Cambridge University Press 1997, pp.173-178

[2] Kolomeitsev L., Kraynov D., Pakhomin F., Rednov F., Kallenbach E., Kireev V., Schneider T., Böcker J. *"Linear Switched Reluctance Motor as High Efficiency Propulsion System for Railway Vehicles"* SPEEDAM 2008 pp 155-160.

[3] Lobo N.S., Honh Sun Lim, Krishnan R. *"Comparison of Linear Switched Reluctance Machines for Vertical* Propulsion *Application: Analysis, Design, and Experimental Correlation"*. IEEE Transactions on Industry Applications, Vol. 44, No 4 July/August 2008, pp 1134-1142

[4] Takeda Y., Morimoto S., Ishikawa S., Hirasa T., Taniguchi K., *"Optimum tooth design for linear pulse motor"*. Industry Applications Society Annual Meeting, 1989., Conference Record of the 1989 IEEE , vol., No., vol.1, pp.272-277

[5] Krishnan, *Switched Reluctance Motor Drives.* CRC Press 2001, pp.138-141.

[6] Rafajdus P., Zrak I., Hrabovcová V., "*Analysis of the Switched Reluctance Motor (SRM) Parameters" Journal of* ELECTRICAL *ENGINEERING*, Vol. 55, No. 7-8, 2004.

[7] Roters H. C. Electromagnetic devices. John Wiley & Sons, Inc. 1941, pp 128-131

[8] T.J.E Miller, "*Optimal Design of Switched Reluctance Motors*". IEEE Transactions on Industrial Electronics, vol. 49, no. 1, pp. 15-27, Feb 2002

[9]. Matveev A, Kuzmichev V., Lomonova E., "*A new comprehensive approach to estimation of end-effects in switched reluctance motors*", Proceedings ICEM2002, Bruges, Belgium, August 2002

[10] Garcia Amorós J., Andrada Gascón P., "*Study of end-effects on the performance of the linear switched reluctance motor*", Proceedings 11th Spanish-Portuguese Conference on Electrical Engineering (11CHLIE), Zaragoza, Spain, July 2009, submitted for publication.

[11] D.C. Meeker, Finite Element Magnetics Method. Version 4.2. 15 May 2008 (*http://femm.foster-miller.net*)

[12] H. Bausch, K. Kanelis, "Feedforward Torque Control of a Switched Reluctance Motor Based on Static Measurement" ETEP, vol. 7, no. 6, pp. 373-380, November/December 1997

Appendix I:
Algorithm for computing the flux linkage – current characteristic

Parameters: c_p, b_p, c_s, b_s, l_s, g, L_W, d_c, N_1, m, *error*,
$BH_{mat}=[B_{mat,1}\ldots B_{mat,z}\ ;\ H_{mat,1}\ldots H_{mat,z}]$
Input: current density range $J=[1\ldots J_{max}]$
Output: flux linkage – current characteristic $\Psi_w = f(I)$

1: $l=[l_1\ \ldots\ l_k]$; $S=[S_1\ \ldots\ S_k]$ *% effective length and sections (see table I)*
2: **for** $j = 1 : J_{max}$ **do**
3: $I(j)=0.25*\pi*d_c^{\,2}*j$
4: $\Phi_A=0$; $\Phi_B=\max(BH_{mat}(1,:))*\max(S)$; $mmf_j=0$;
5: **while** $|\ N_1*I(j) - mmf_j\ | > error$ **do**
6: $\Phi_{1,j}=0.5*(\ \Phi_A + \Phi_B)$
7: $B_1= \Phi_{1,j} / S_1$; $H_1=$ interpolation(BH_{mat} , B_1)
8: $B_5= \Phi_{1,j} / S_5$; $H_5=$ interpolation(BH_{mat} , B_5)
9: $\theta_{AC}=N_1*I(j)*\alpha_p - H_1*l_1 - H_5*l_5$
10: $\Phi_{3,j}=\theta_{AC} / R_7$
11: $\Phi_{2,j}=|\Phi_{1,j} - \Phi_{3,j}|$
12: $B_2= \Phi_{2,j} / S_2$; $H_2=$ interpolation(BH_{mat} , B_2)
13: $B_6= \Phi_{2,j} / S_6$; $H_6=$ interpolation(BH_{mat} , B_6)
14: $B_4= \Phi_{2,j} / S_4$; $H_4=$ interpolation(BH_{mat} , B_4)
15: $B_3= \Phi_{2,j} / S_3$; $H_3= B_3 / \mu_0$
16: $mmf_j = H_1*l_1 + H_2*l_2 + H_3*l_3 + 0.5*H_4*l_4 + H_5*l_5 + 0.5*H_6*l_6$
17: **if** $(N_1*I(j) - mmf_j)>0$ **then** $\Phi_A= \Phi_{1,j}$ **else** $\Phi_B= \Phi_{1,j}$ **end**
18: **end**
19: $\Psi_p\ (j) = \Phi_{1,j} *4*N_1$
20: $\Psi_s\ (j) = \Phi_{2,j} *4*N_1$
21: $\Psi_d\ (j) = \Phi_{3,j} *4*N_1$
22: $\Psi_w\ (j) = \alpha_p*\ \Psi_p\ (j) + (1 - \alpha_p)*\ \Psi_s\ (j)$
23: **end**
24: $\Psi_w I=[I;\ \Psi_w]$

Appendix II:

LSRM prototype main dimensions

	SYMBOL	VALUE (UNITS)
Number of phases	m	4
Stator pole width	b_p	6 (*mm*)
Stator slot width	c_p	6 (*mm*)
Stator pole pitch	T_p	12 (*mm*)
Number of active poles per side (stator)	N_p	8
Stator pole length	l_p	30 (*mm*)
Translator pole width	b_s	7 (*mm*)
Translator slot width	c_p	9 (*mm*)
Translator pole pitch	T_p	16 (*mm*)
Number of passive poles per side (translator)	N_s	6
Translator pole length	l_s	7 (*mm*)
Yoke height	h_y	8 (*mm*)
Stack length	L_W	30 (*mm*)
Air gap length	g	0.5 (*mm*)
Stroke	PS	4 (*mm*)
Number of turns per pole	N_1	11
Wire diameter	d_c	2.1 (*mm*)